Supplementary Information (SI) for Energy & Environmental Science.

Supporting Information

High-performance inverted perovskite solar cells and modules via aminothiazole passivation

Zewei Zhu[1,2#], Bingcan Ke[1,2#], Kexuan Sun[3#], Chengkai Jin[1], Zhenhua Song[3], Ruixuan Jiang[1], Jing Li[1], Song Kong[1], Chang Liu[3], Sai Bai[4], Sisi He[5], Ziyi Ge[3], Fuzhi Huang[1,2*], Yi-Bing Cheng[1,2], Tongle Bu[1*]*

[1]*State Key Laboratory of Advanced Technology for Materials Synthesis and Processing, Wuhan University of Technology, Wuhan 430070, PR China.*

[2]*Xianhu Laboratory of the Advanced Energy Science and Technology Guangdong Laboratory, Foshan 528200, PR China.*

[3]*Zhejiang Provincial Engineering Research Center of Energy Optoelectronic Materials and Devices, Ningbo Institute of Materials Technology & Engineering, Chinese Academy of Sciences, Ningbo 315201, PR China.*

[4]*Institute of Fundamental and Frontier Sciences, University of Electronic Science and Technology of China, Chengdu 611731, PR China.*

[5]*Shenzhen Key Laboratory of Intelligent Robotics and Flexible Manufacturing Systems, Department of Mechanical and Energy Engineering, SUSTech Energy Institute for Carbon Neutrality, Southern University of Science and Technology, Shenzhen, 518055, PR China.*

[#]*These authors contributed equally to this work*

***Corresponding authors**. Email: tongle.bu@whut.edu.cn; fuzhi.huang@whut.edu.cn; liuchang1@nimte.ac.cn*

EXPERIMENTAL METHODS

Materials

(4-(3,6-diphenyl-9H-carbazol-9-yl)butyl)phos phonic (Ph-4PACz, 98.0%), cesium iodide (CsI, 99.99%), formamidinium iodide (FAI, 99.5%), methylammonium iodide (MAI, 99.5%), phenylethylammonium bromide (PEABr, 99.5%), 2-(4-(Trifluoromethyl)phenyl)ethan-1-aminium Iodide (CF_3-PEAI, 99%), fullerene-C_{60} (C_{60}, 99%), and bathocuproine (BCP, 99%) were obtained from Xi'an Yuri Solar Co., N, N-dimethylformamide (DMF, 99.9%), dimethyl sulfoxide anhydrous (DMSO, 99.9%), ethyl alcohol (EtOH, 99.5%), chlorobenzene (CBZ, 99.5%) and ethyl Acetate anhydrous (EA, 99.8%) were supplied by Sigma-Aldrich. 5-thiazolamine hydrochloride (5ATCl, 99%) was provided by Aladdin.

Fabrication of the rigid and flexible PSCs

Rigid glass/FTO and flexible PET/ITO substrates were washed before use. A monolayer of Ph-4PACz was deposited onto the substrates as the hole transport layer (HTL) by spin-coating at 3000 rpm for 30 s, followed by annealing at 100 °C for 10 min. The Ph-4PACz precursor solution was prepared by dissolving 0.5 mg of Ph-4PACz in 1 mL of ethyl alcohol. The $Cs_{0.05}FA_{0.85}MA_{0.1}PbI_3$ perovskite was prepared by mixing CsI (19.5 mg), MAI (23.8 mg), FAI (219.3 mg), and PbI_2 (726.5 mg) with an additional addition 15% MACl and 0.5% RbI in mixed solutions (DMF: DMSO = 5:1 in volume ratio, 1 mL). For the fabrication of perovskite films, the perovskite films were spin-coated onto the FTO/ Ph-4PACz substrates at 1000 rpm for 10 s and 5000 rpm for 35 s. Chlorobenzene (130 μL) was dropped at the center of the spinning substrate approximately 15s before the end of the spin coating procedure. The samples were then annealed at 100 °C for 30 min in the nitrogen glovebox. After cooling, the passivation layers of PEABr and CF_3-PEAI were sequentially spin-coated on the perovskite surface at 5000 rpm for 30 s and thermal annealing at 100 ℃ for 5 min, respectively. Finally, C_{60} (25 nm), BCP (7 nm), and Ag (100 nm) were successively thermally evaporated to complete the fabrication of PSCs, which were evaporated using a PD-400S vacuum evaporation system (PDVACUUM).

Fabrication of the rigid solar mini-modules

First, The FTO substrate was pre-scribed using a picosecond laser for the P1 patterns with a width of ~20 μm, and the distance between each P1 pattern is 6.7 mm. The subsequent processes for the preparation of the Ph-4PACz layer, perovskite layer, passivation layers, C_{60} layer, and BCP layer are similar to the small-area devices. Then, the as-deposited substrates were scribed to form the P2 patterns with a width of ~170 μm. Finally, when a 100 nm-thick Ag layer is deposited, the substrate is further scribed to form the P3 patterns with a width of ~50 μm, thus completing the series-connected solar mini-module fabrication. The series interconnection of the module was realized by P1, P2, and P3 lines, which were patterned using a PLSS10 laser scribing system (Microtreat), The corresponding detailed scribing design of the mini-module is shown in Fig S19.

Characterizations

The morphologies and cross-section SEM images of perovskite films were characterized by field-emission scanning electron microscopy (FE-SEM, HITACHI S-4800). The crystallinity of the perovskite films was analyzed using an X-ray diffractometer (XRD, D8 Advance). Grazing-incidence wide-angle X-ray scattering (GIWAXS) and Grazing Incidence X-ray diffraction (GIXRD) measurements were performed by Xeuss 3.0 SAXS/WAXS (the detector model is Eiger2R 1M) with a copper target 8.05 KeV X-ray was used, and the wavelength is 1.54189 Å (Test environment: Vacuum< 1 mbar). Ultraviolet photoelectron spectroscopy (UPS) and X-ray photoelectron spectroscopy (XPS) were performed using an AXIS SUPRA instrument (Shimadzu). Steady-state photoluminescence (PL) spectra were recorded with an Ocean Insight spectrometer under a 405 nm excitation source, while time-resolved photoluminescence (TRPL) measurements were conducted with a HORIBA Scientific Nano LED-C2 N-485L system under a 485 nm excitation source. The photoluminescence quantum yield (PLQY) of perovskite films was determined using a 405 nm laser source (EnliTech). Femtosecond transient absorption spectroscopy (TAS) measurements were carried out using a SOL-F-K-HP-T setup with a 400 nm pump wavelength. The Atomic force microscopy (AFM) and Kelvin probe force microscopy (KPFM) images were obtained by Dimension ICON SPM (Dimension Icon, German). Fourier-transform infrared (FTIR) spectra were conducted with a Nexus spectrometer, while nuclear magnetic resonance (NMR) spectroscopy was measured by a Bruker Advance III HD 500 MHz system. The device performance was measured under AM 1.5G illumination using a solar simulator (SS-XRC, Enlitech) calibrated to an intensity of 100 mW cm^{-2} with a reference silicon solar cell. External quantum efficiency (EQE) spectra were acquired with a computer-controlled QE-R system (Enlitech).

Theoretical Calculation:

The DFT calculations in this research are performed using the Vienna ab initio simulation software (VASP)[1]. To simulate electron exchange-related interactions, the Perdew–Burke–Ernzerhof (PBE)[2] functional is utilized, and the projector augmented wave (PAW)[3] approach is used for electron-ion–nucleus interactions. In order to handle van der Waals interactions in perovskites, we employ the Grimme DFT-D3 approach with Becke-Johnson damping[4, 5]. Geometry optimization is carried out with the Γ-centered 2×2×1 Monkhorst−Pack k-point mesh and the 400eV plane wave energy cutoff. The geometric structure is regarded as convergent when the energy difference between all ions is smaller than -10^{-4}eV.

Based on the structurally optimized model, the corresponding defect models (V_I, V_{Pb}, I_{Pb}, I_I) were established. The defect formation energies can be obtained using the defect energy calculation formula:

$$\Delta H_{D,q}(E_F,\mu) = [E_{D,q} - E_H] + \sum_i n_i\mu_i + qE_F + E_{corr}$$

Where D represents the dopant element, and q is the number of gained or lost electrons. $E_{D,q}$ is the total energy of the charged defect system, and E_H is the total energy of the pre-doped structure. The term $\sum_i n_i\mu_i$ represents the chemical potential contribution of atoms, relative to the complete bulk structure. Here, n_i is the difference in the number of atoms, where $n_i < 0$ corresponds to the addition of atoms, and μ_i is the chemical potential of the atoms. The term qE_F accounts for the contribution due to the different number of electrons, where $q > 0$ indicates a decrease in the number of electrons in the system, and $q < 0$ indicates an increase in electrons, with E_F being the Fermi level. E_{corr} is the correction for the charged system.

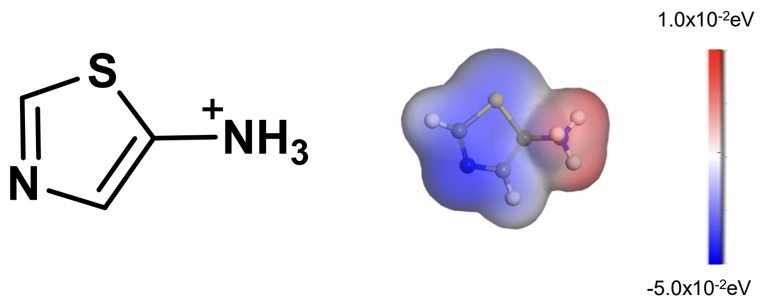

Fig S1. The molecular structure and electrostatic potential (φ) of 5ATCl.

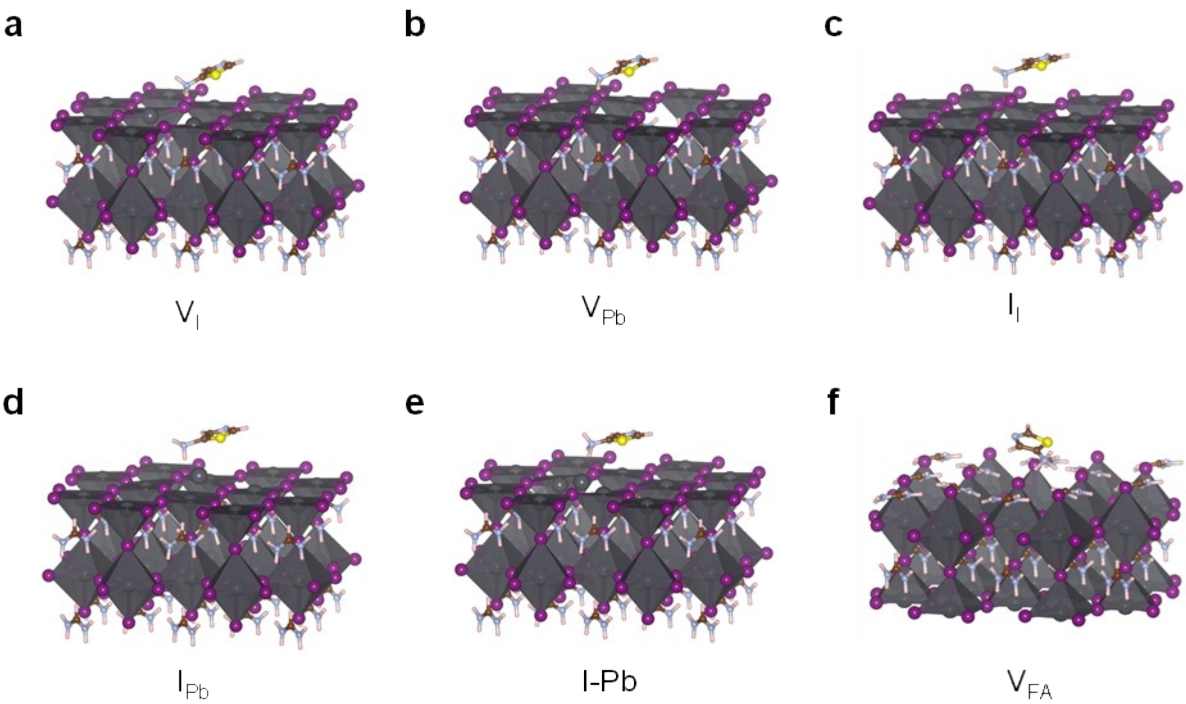

Fig S2. The defect models of perovskite after adsorbing with 5ATCl. (a) I vacancy, (b) Pb vacancy, (c) I interstitial, (d) Pb interstitial, (e) I-Pb substitutional, and (f) FA vacancy.

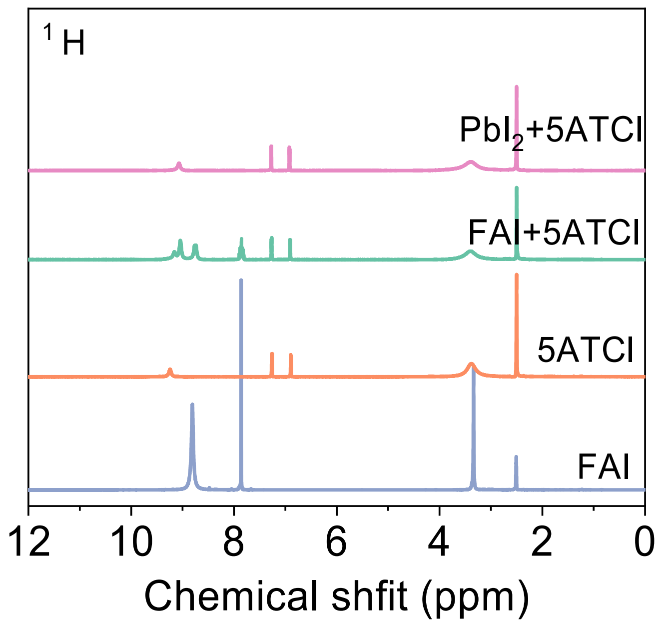

Fig S3. Full NMR spectra of FAI, 5ATCl, FAI mixed with 5ATCl, and PbI_2 mixed with 5ATCl in DMSO-d_6 solutions.

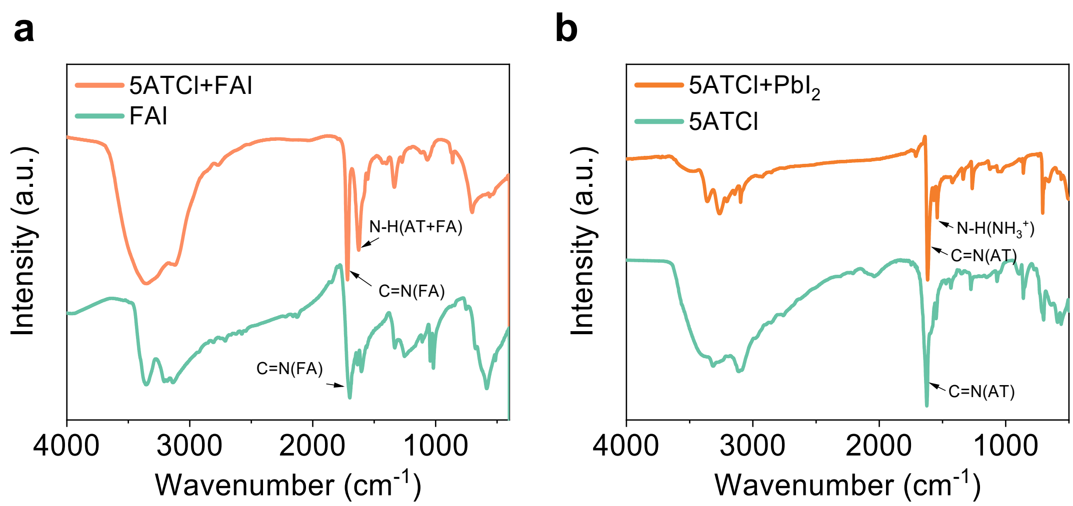

Fig S4. FTIR spectra of (a) FAI and 5ATCl+FAI films. (b) FTIR spectra of 5ATCl and 5ATCl+PbI_2 films.

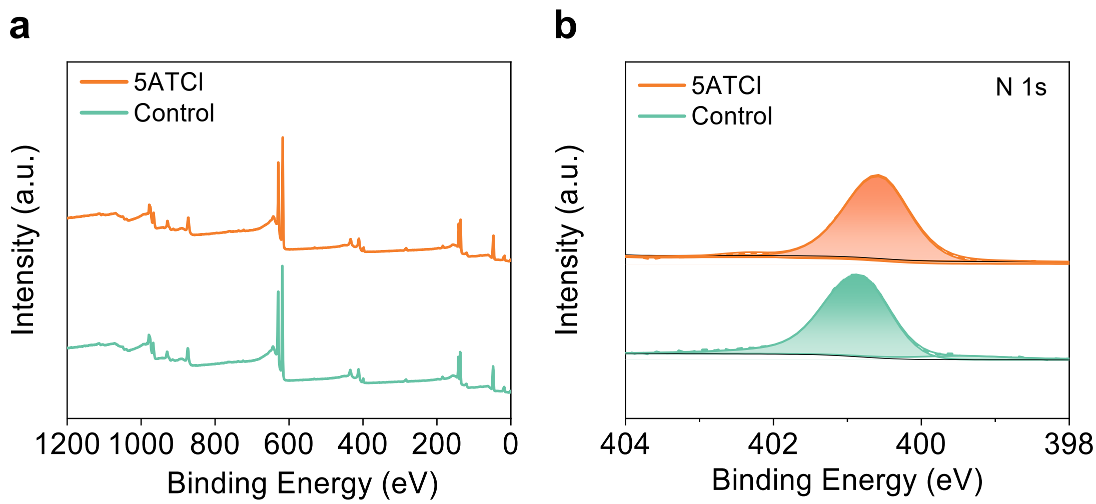

Fig S5. (a) Full XPS spectra of the control and the 5ATCl-modified perovskite films. (b) High-resolution XPS spectra of N 1s for the control and the 5ATCl-modified perovskite films.

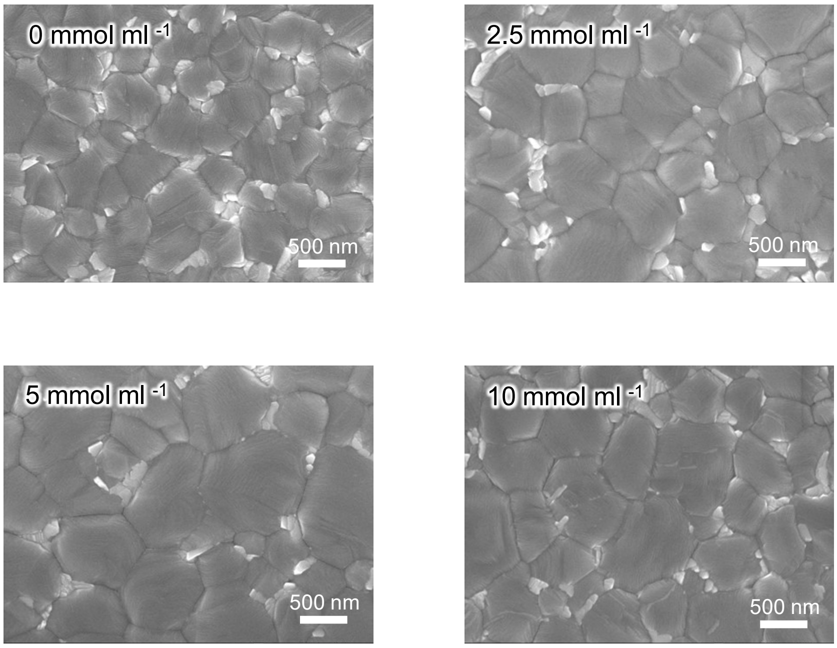

Fig S6. SEM images of perovskite films fabricated with different concentrations of 5ATCl.

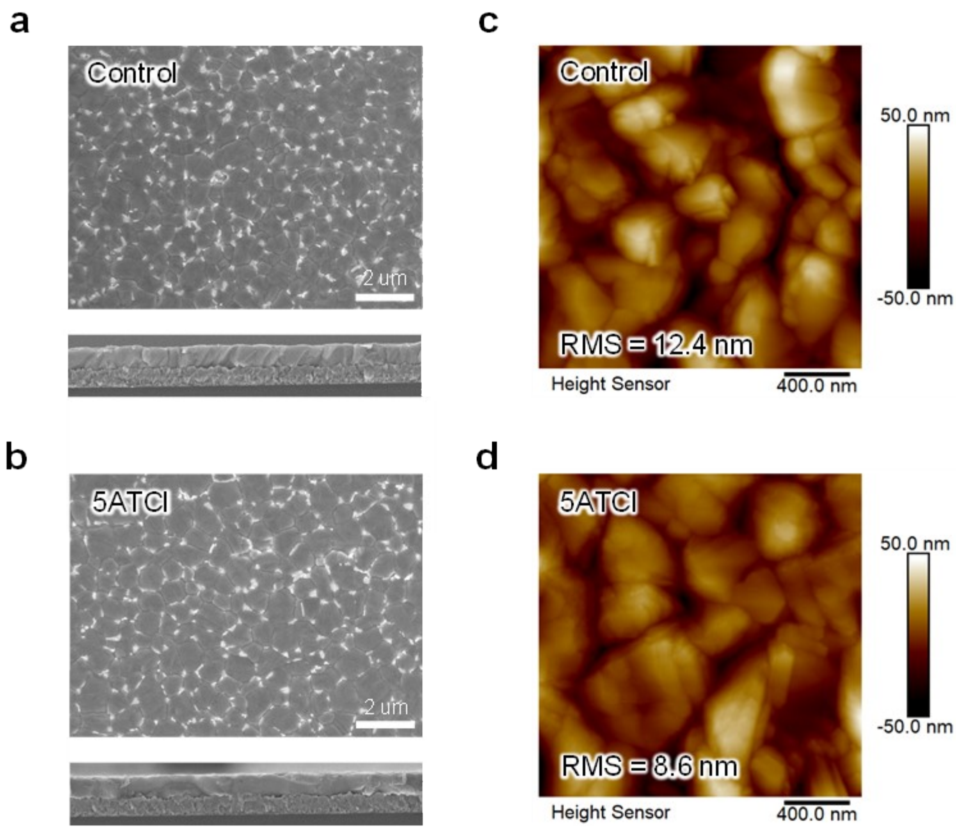

Fig S7. SEM images with low magnification for (a) the control and (b) the 5ATCl-modified perovskite films. AFM images of (c) the control and (d) the 5ATCl-modified perovskite films.

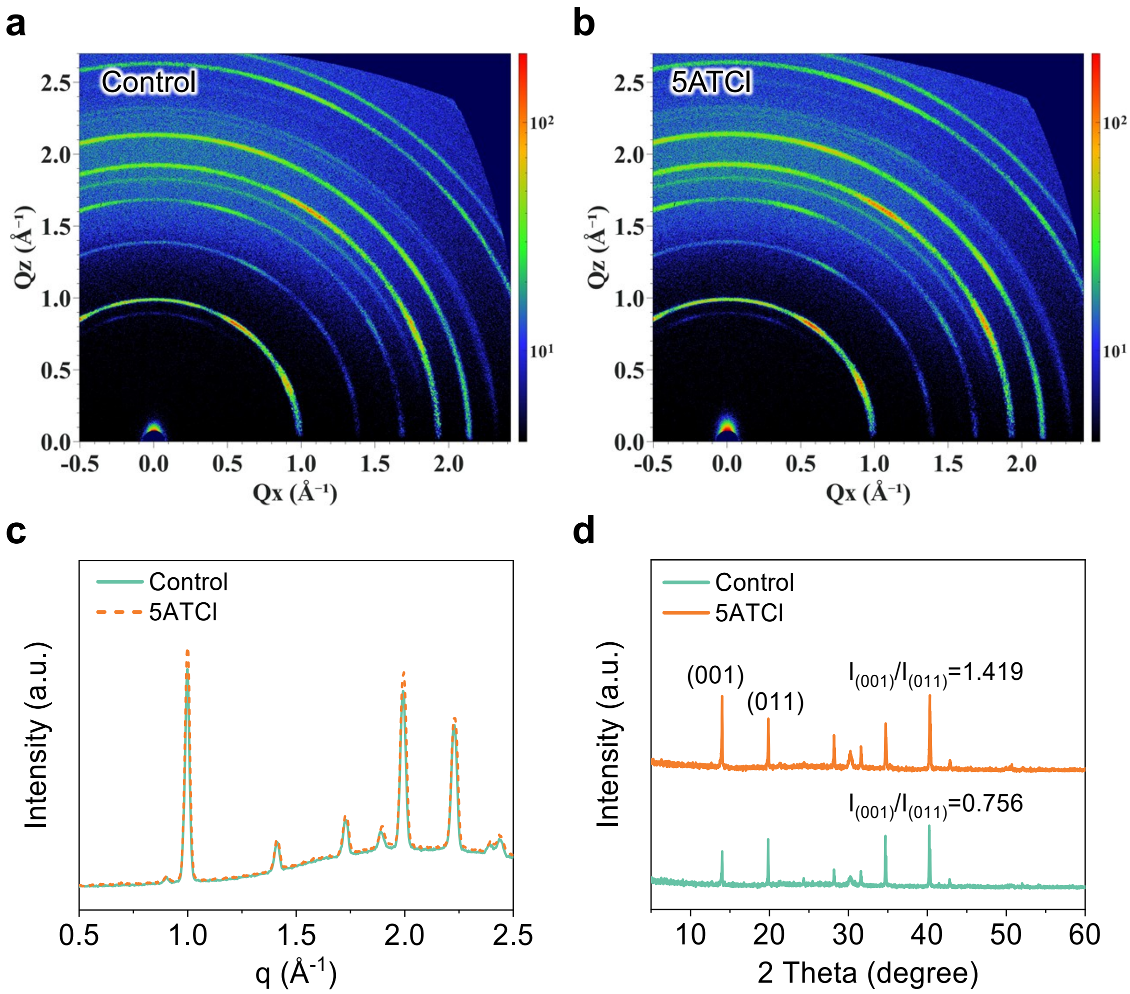

Fig S8. 2D GIWAXS data of (a) the control and (b) the 5ATCl-modified perovskite films. (c) 1D out-of-plane radial cake cut profiles of the control and the 5ATCl-modified perovskite films. (d) XRD patterns of the control and the 5ATCl-modified perovskite films.

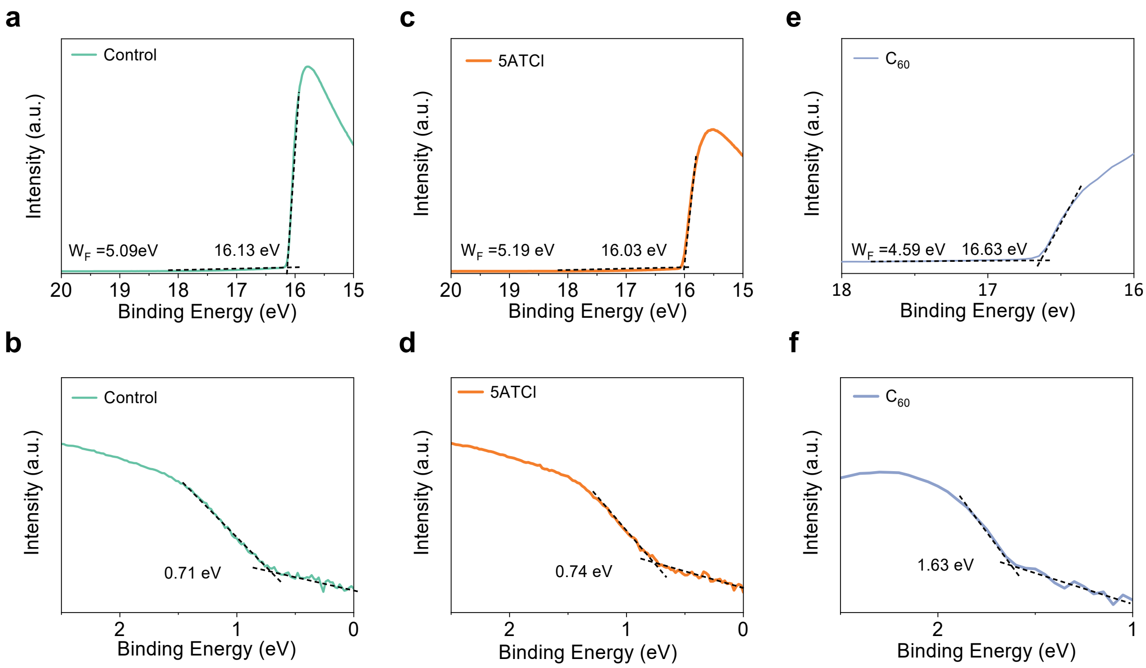

Fig S9. UPS spectra of the control perovskite film (a, b), the 5ATCl-modified perovskite film (c, d), and C_{60} film (e, f).

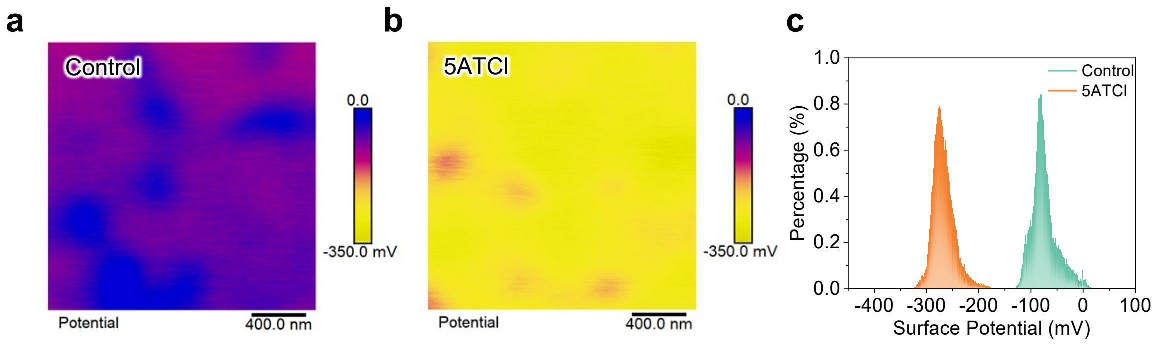

Fig S10. KPFM surface potential images of (a) the control and (b) the 5ATCl-modified perovskite films. (c) The corresponding CPD distribution.

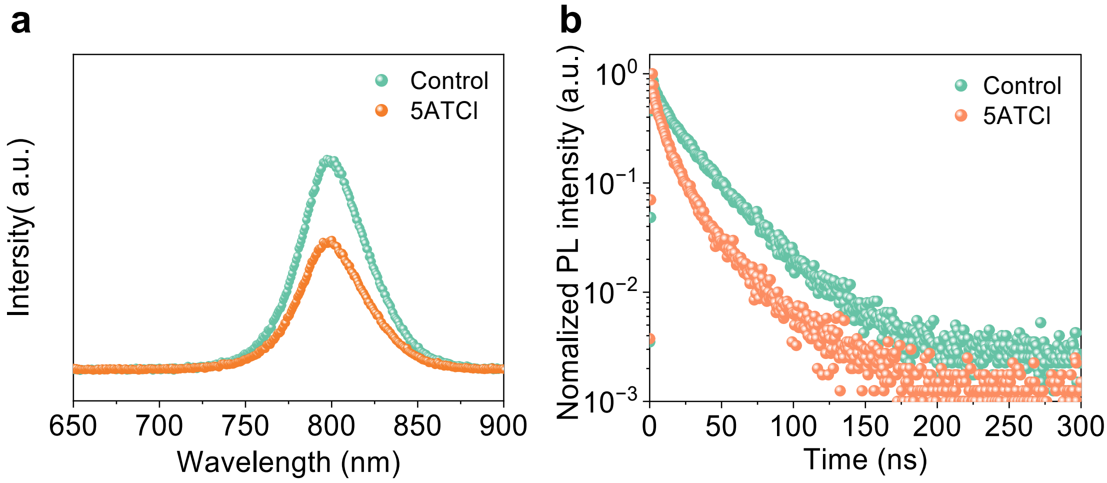

Fig S11. (a) Steady-state PL and (b) TRPL decays of control and 5ATCl treated glass/perovskite/C_{60} stacks.

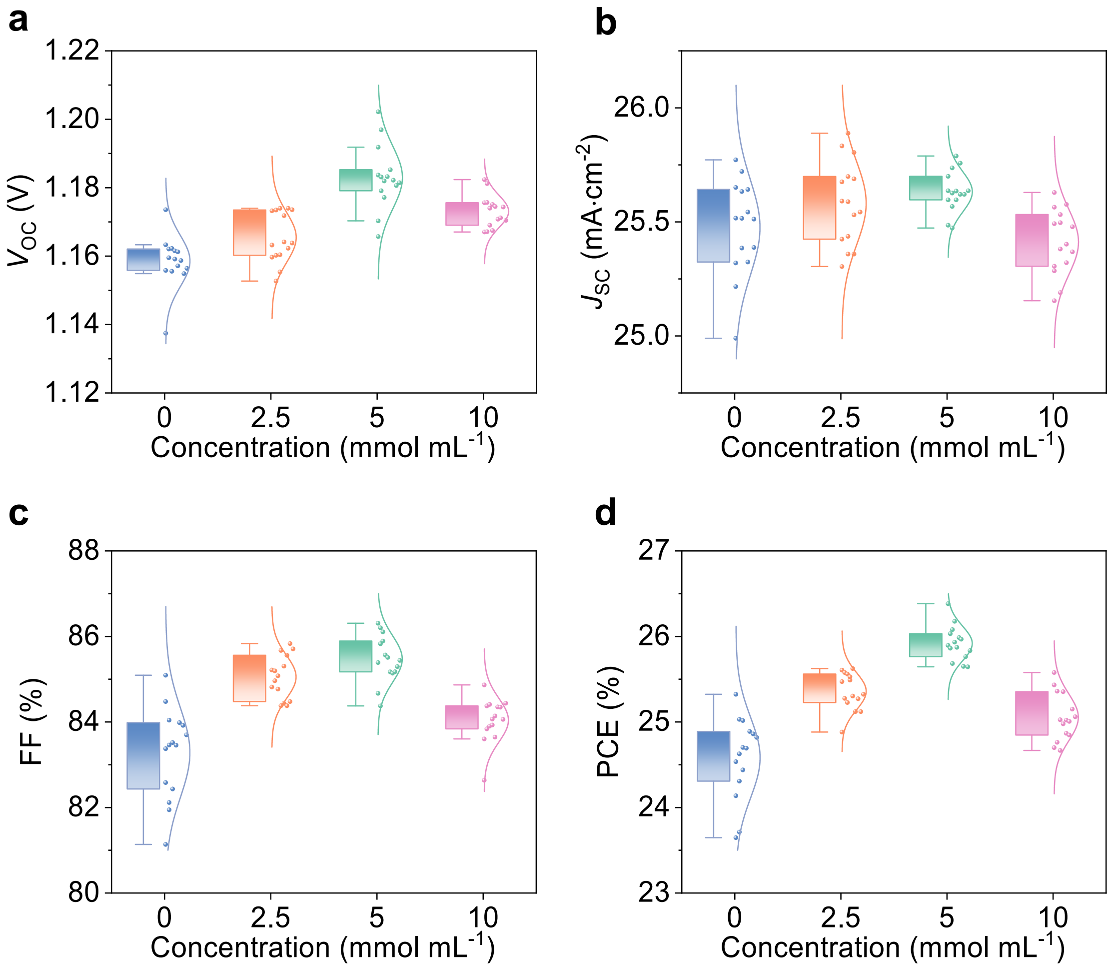

Fig S12. Statistic box plots of *J-V* parameters for devices under different concentrations of 5ATCl. (a) V_{OC}, (b) J_{SC}, (c) FF, and (d) PCE.

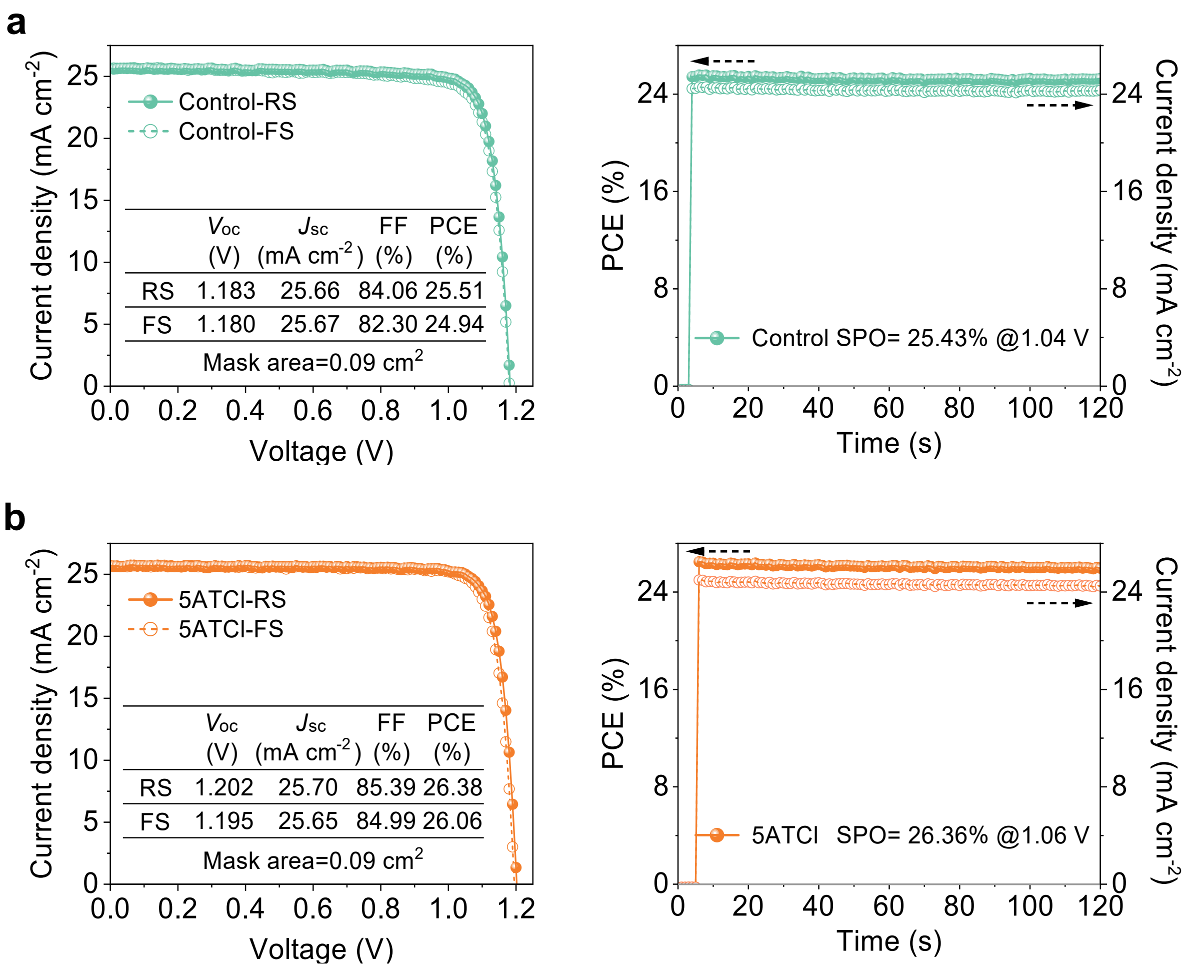

Fig S13. Champion *J-V* curves and SPO curves of (a) the control and (b) the 5ATCl-modified rigid PSCs.

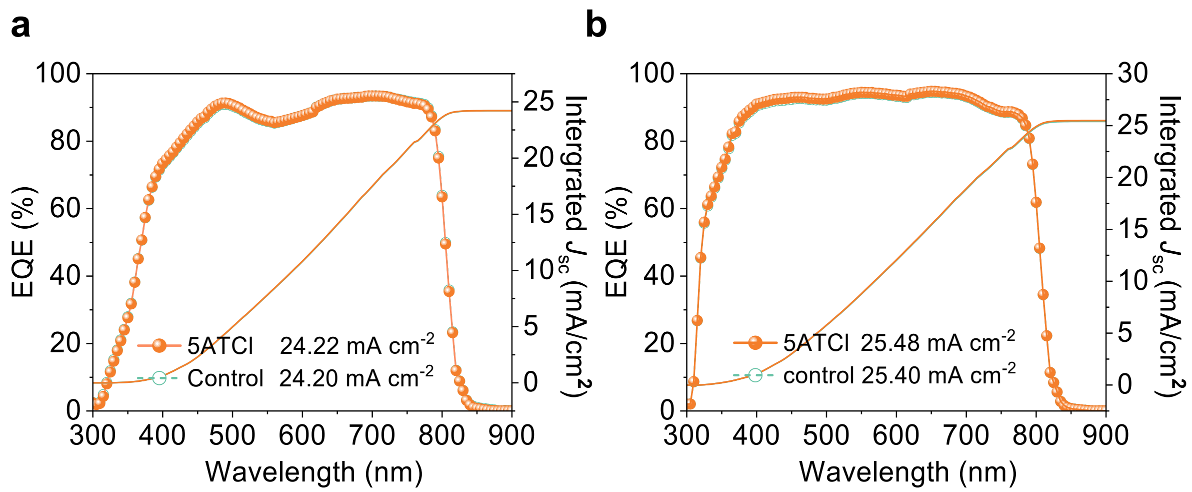

Fig S14. EQE spectra of the control and the 5ATCl-modified PSCs with anti-reflection coating. (a) Flexible PSCs, (b) rigid PSCs.

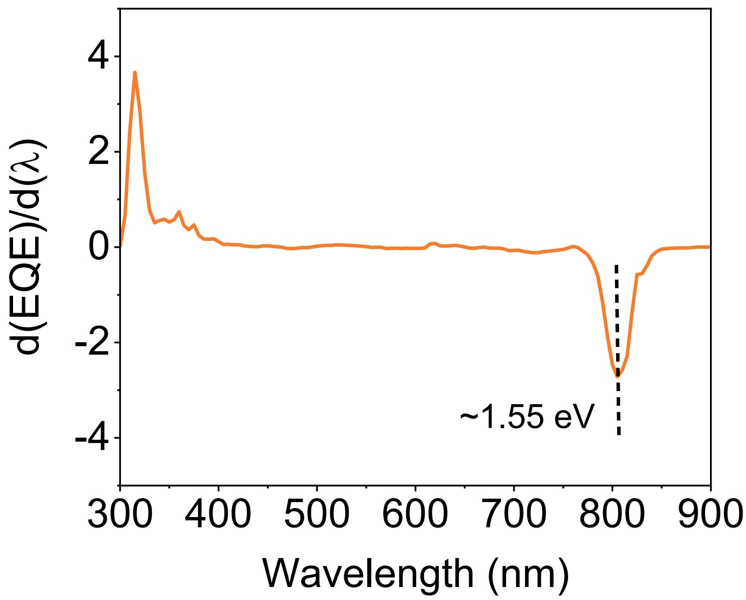

Fig S15. Differential plot from EQE spectrum of the 5ATCl-modified PSC.

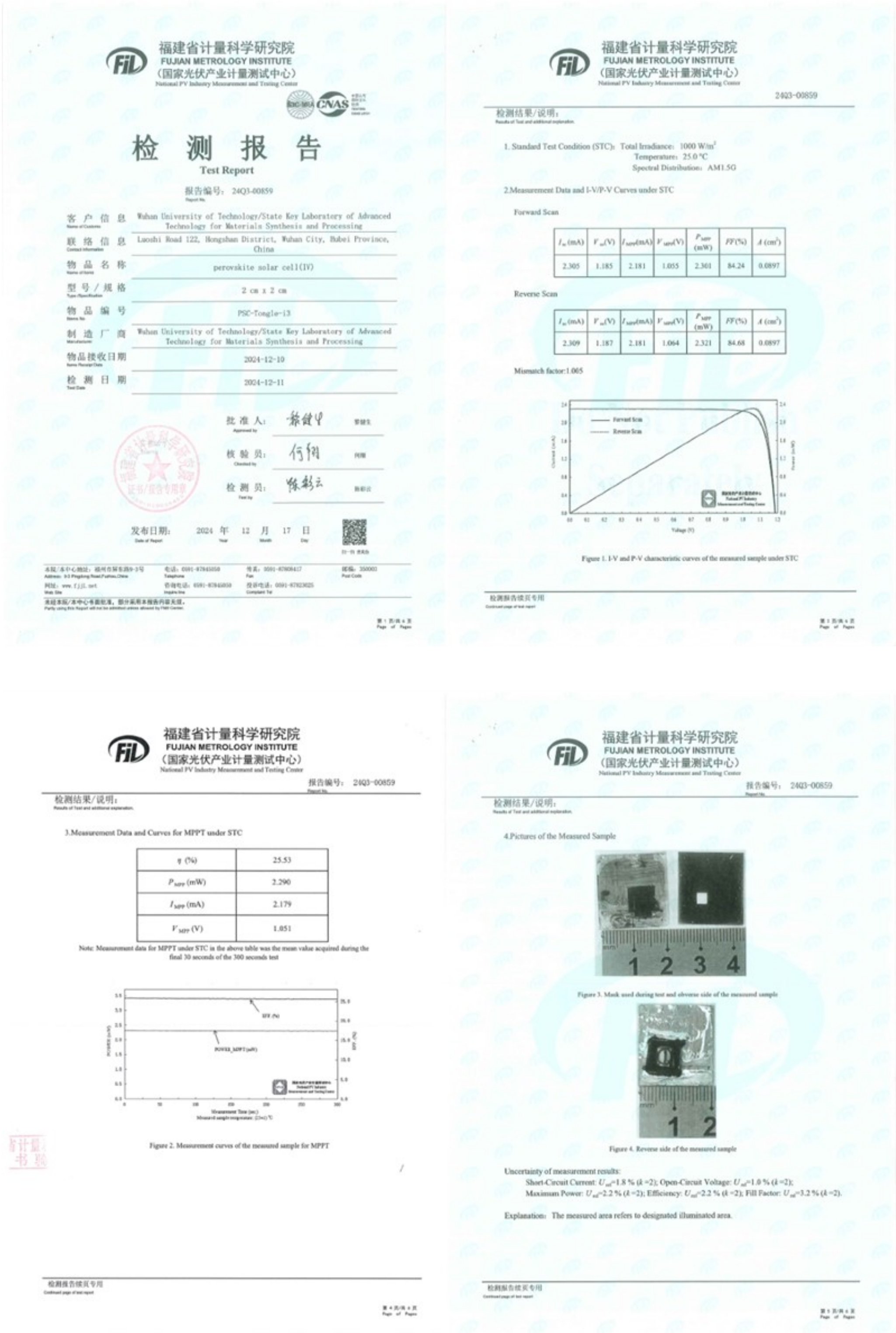

Fig S16. Small-sized devices certification report. Certificate of a small-sized perovskite solar cell based on 5ATCl modification (Certification Authority Center: National PV Industry Measurement and Testing Center.). The PCEs are 25.87% and 25.65% under reverse and forward scans, and the corresponding SPO is 25.53%, respectively.

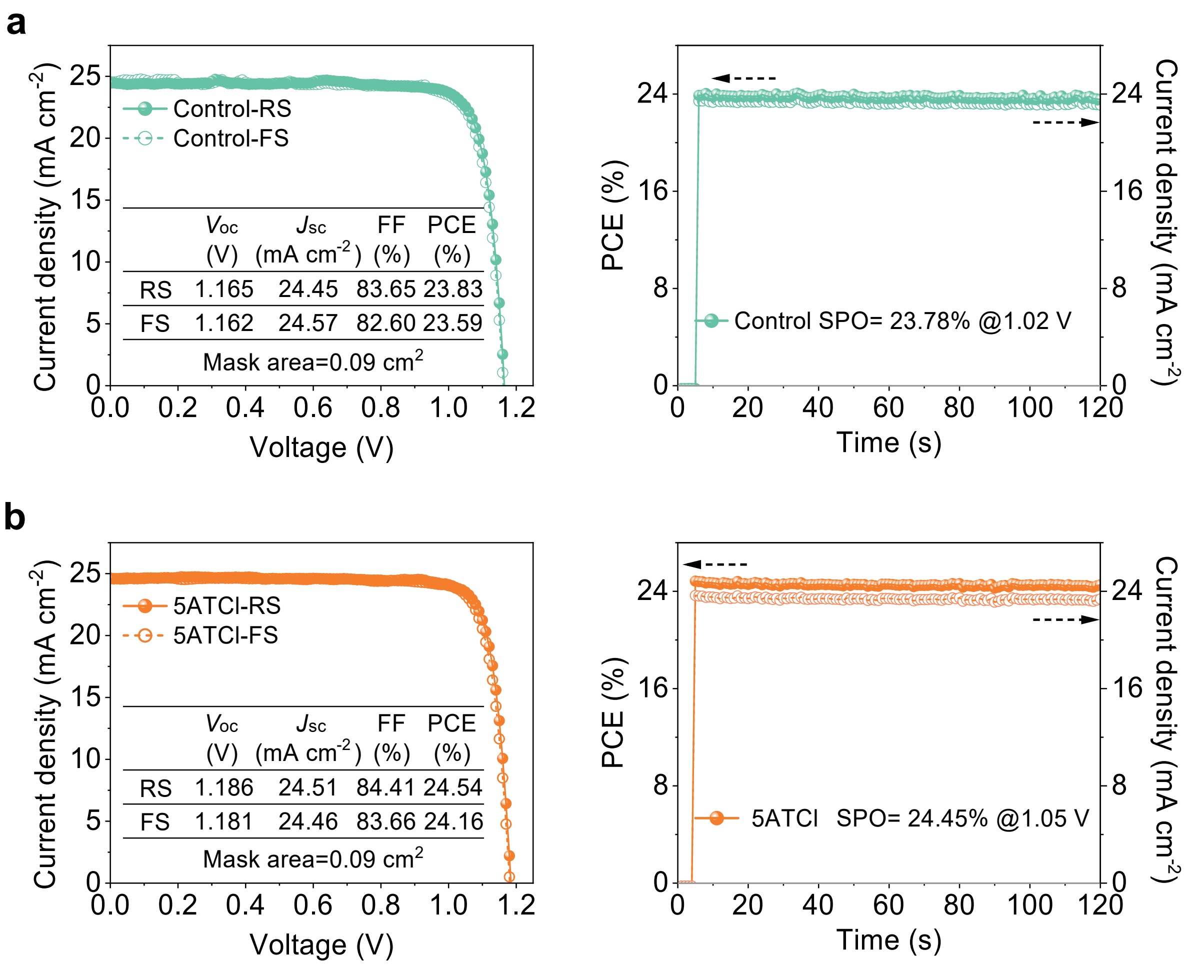

Fig S17. Champion *J-V* curves and SPO curves of (a) the control and (b) the 5ATCl-modified flexible PSCs.

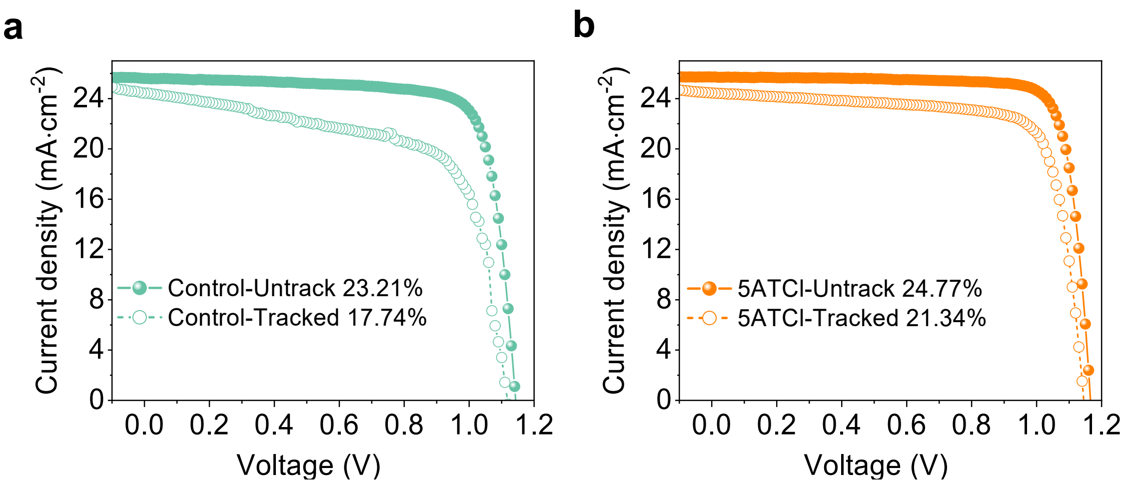

Fig S18. The *J-V* curves of (a) the control and (b) the 5ATCl-modified PSCs before and after 1100 hours of maximum power point tracking.

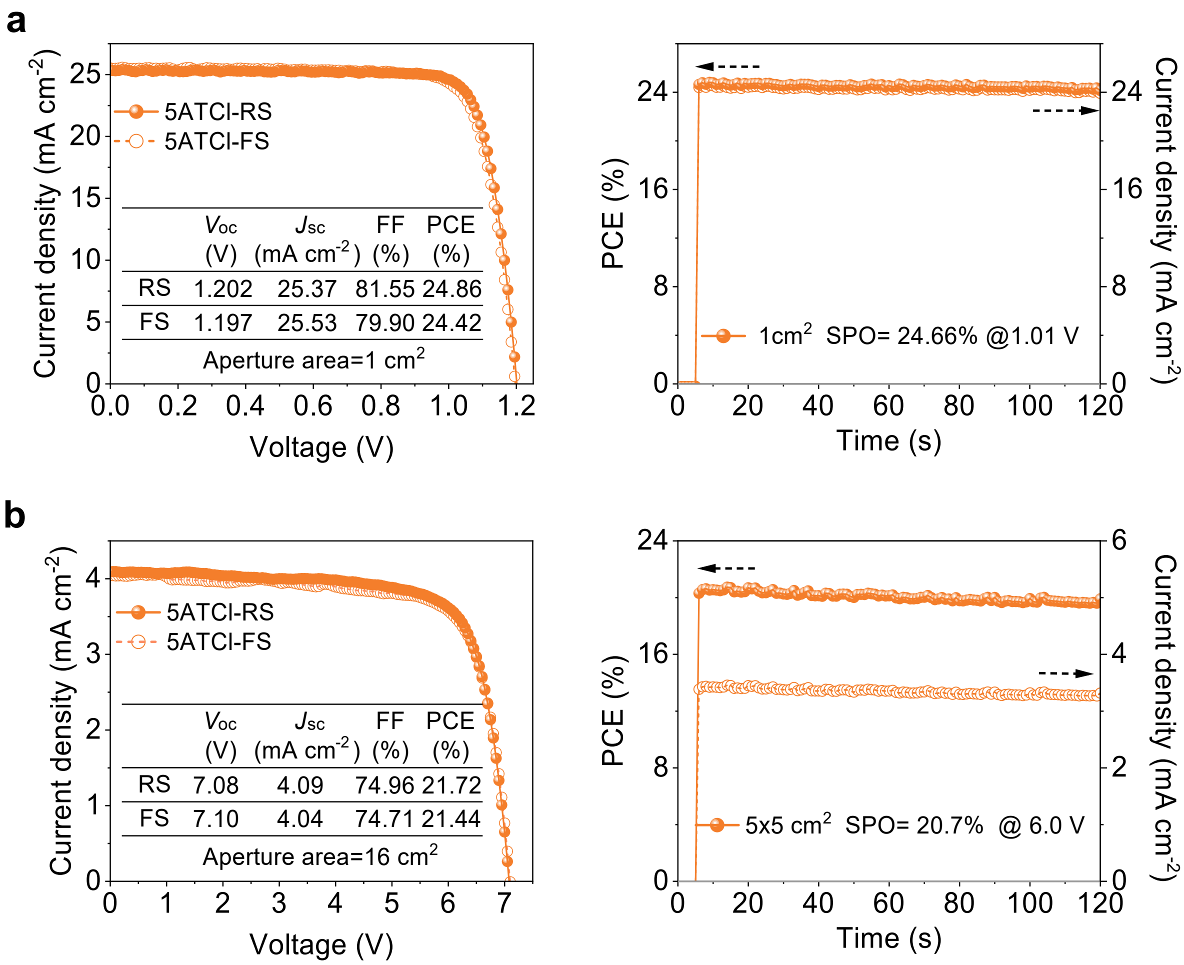

Fig S19. Champion *J-V* curves and SPO curves of (a) the 5ATCl-modified 1 cm^2 large-size PSCs, and (b) the 5ATCl-modified 5 cm × 5 cm solar mini-module.

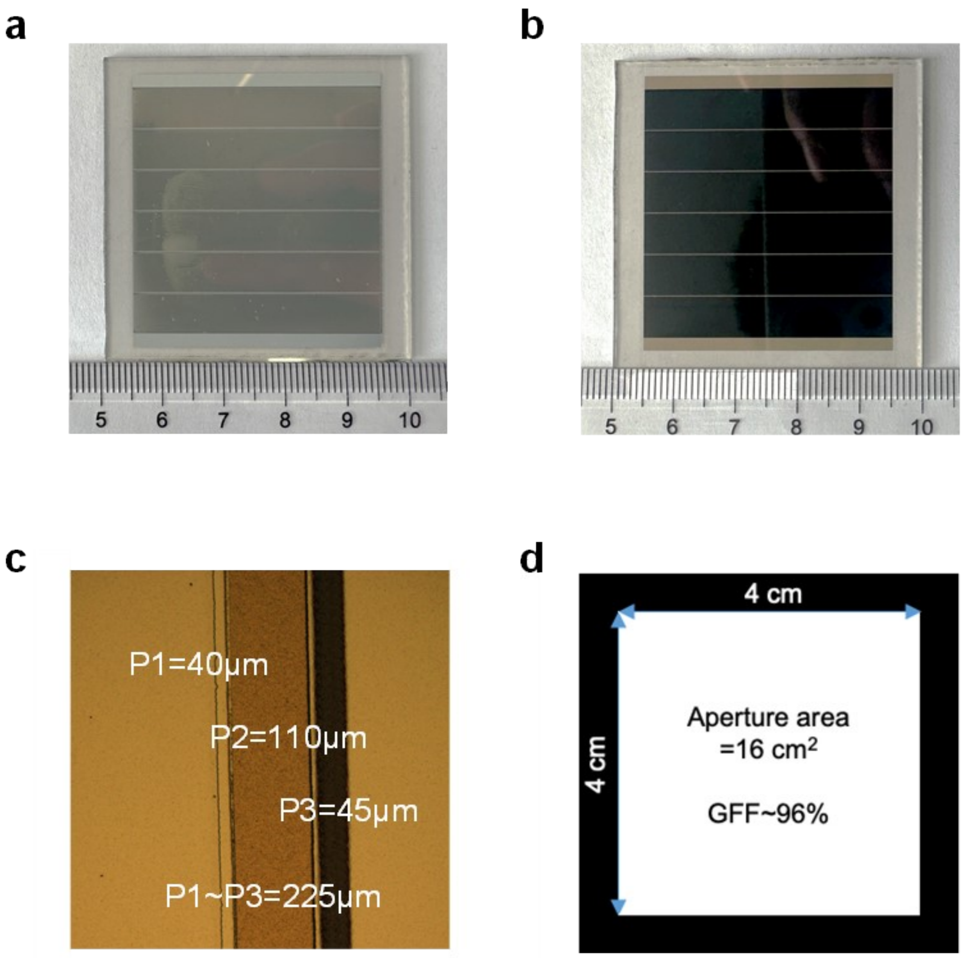

Fig S20. Design of the module and corresponding test mask. (a) Front-side view and (b) back-side view photographs of a 5 cm × 5 cm perovskite solar mini-module. (c) The optical image of the P1-P2-P3 patterning of the mini-module. (d) The metal mask was used for the test with an aperture area of 16 cm^2.

Table S1. TAS fit parameters of the perovskite films with 5ATCl a structure of glass/perovskite. The laser incidents from the perovskite side.

Film	τ_1 (ps)	τ_2 (ps)	A_1 (%)	A_2 (%)	τ_{ave} (ps)
Control	1.62	130.69	74.71	25.29	126.13
5ATCl	10.16	514.70	55.09	44.91	502.77

Table S2. TRPL fit parameters of the perovskite films with 5ATCl a structure of glass /perovskite. The laser incidents from the perovskite side.

Film	τ_1 (ns)	τ_2 (ns)	A_1 (%)	A_2 (%)	τ_{ave} (ns)
Control	137.62	639.17	25.1	73.9	605.41
5ATCl	139.44	701.25	23.15	76.85	695.32

Table S3. TRPL fit parameters of the perovskite films with 5ATCl a structure of glass /perovskite/C_{60}. The laser incidents from the perovskite side.

Film	τ_1 (ns)	τ_2 (ns)	A_1 (%)	A_2 (%)	τ_{ave} (ns)
Control	4.8	18	23.3	76.7	17.01
5ATCl	4.32	15.63	41.81	58.19	13.75

Table S4. The performance parameters of the *J-V* test were conducted on the champion of the control and 5ATCl-modified rigid devices.

Devices	Sweep direction	V_{OC} (V)	J_{SC} (mA cm^{-2})	FF (%)	PCE (%)
R-PSCs-Control	RS	1.183	25.66	84.06	25.51
R-PSCs-Control	FS	1.180	25.67	82.30	24.94
R-PSCs-5ATCl	RS	1.202	25.70	85.39	26.38
R-PSCs-5ATCl	FS	1.195	25.65	84.99	26.06

Table S5. The performance parameters of the *J-V* test were conducted on the champion of the control and 5ATCl-modified flexible devices.

Devices	Sweep direction	V_{OC} (V)	J_{SC} (mA cm^{-2})	FF (%)	PCE (%)
F-PSCs-Control	RS	1.165	24.45	83.65	23.83
F-PSCs-Control	FS	1.162	24.57	82.60	23.59
F-PSCs-5ATCl	RS	1.186	24.51	84.41	24.54
F-PSCs-5ATCl	FS	1.181	24.46	83.44	24.16

Table S6. Photovoltaic parameters derived from the *J-V* curves of high-efficiency PSCs reported in recent years.

Type	Configuration	J_{SC} (mA cm^{-2})	V_{OC} (V)	FF (%)	PCE (%)
p-i-n	FTO/Me-4PACz/Perovskite/C_{60}/BCP/Ag	25.67	1.178	86.47	26.15[6]
n-i-p	FTO/TiO_x/Perovskite/Spiro-OMeTAD/Au	26.47	1.175	84.94	26.41[7]
n-i-p	FTO/SnO_2/Perovskite/Spiro-OMeTAD/Au	26.27	1.175	85.90	26.51[8]
n-i-p	FTO/SnO_2/Perovskite/Spiro-OMeTAD/Au	26.39	1.171	85.42	26.4[9]
p-i-n	FTO/2PACz+Me-4PACz/Perovskite/C_{60}/BCP/Ag	26.40	1.18	86.2	26.9[10]
p-i-n	FTO/SAMs/Perovskite/C_{60}/SnO_2/Ag	26.10	1.17	85.2	26.15[11]
n-i-p	ITO/SnO_2/Perovskite/Spiro-OMeTAD/Au	26.23	1.187	84.55	26.32[12]
n-i-p	FTO/SnO_2/Perovskite/Spiro-OMeTAD/Au	26.21	1.18	83.73	26.03[13]
p-i-n	FTO/2PACz+Me-4PACz/Perovskite/C_{60}/BCP/Ag	26.5	1.18	85.5	26.7[14]
p-i-n	ITO/NiO_x/NA-Me-4PACz/Perovskite/PCBM/BCP/	26.3	1.203	84.5	26.69[15]

	Ag				
p-i-n	ITO/NiO_x/PTAA/Perovskite/PCBM/BCP/Ag	26.07	1.182	84.7	26.1[16]
p-i-n	ITO/4PADCB/Perovskite/C_{60}/BCP/Cu	25.84	1.184	85.8	26.27[17]
p-i-n	ITO/HTMs/Perovskite/C_{60}/BCP/Ag	25.65	1.178	86.2	26[18]
p-i-n	FTO/ SAMs/Perovskite/C_{60}/SnO_2/Ag	26.18	1.194	85.76	26.81[19]
This work*	FTO/Ph-4PACz/Perovskite/C_{60}/BCP/Ag	25.70	1.202	85.39	26.38

Table S7. Photovoltaic parameters derived from the *J-V* curve of PCE exceeding 24% flexible PSCs reported in recent years.

Type	Configuration	J_{SC} (mA cm^{-2})	V_{OC} (V)	FF (%)	PCE (%)
p-i-n	PEN/ITO/A-4PADCB/Perovskite/C_{60}/BCP/Ag	25.39	1.186	83.14	25.05[20]
n-i-p	PET/ITO/SnO_2/Perovskite/Spiro-OMeTAD/Au	25.18	1.18	82.4	24.47[21]
n-i-p	PET/ITO/SnO_2/Perovskite/Spiro-OMeTAD/Au	25.4	1.17	83.9	24.9[22]
n-i-p	PET/ITO/SnO_2/Perovskite/Spiro-OMeTAD/Au	24.96	1.173	83.51	24.45[23]
p-i-n	PEN/ITO/Meo-2PACz/Perovskite/C_{60}/BCP/Ag	25.3	1.14	84	24.08[24]
n-i-p	PET/ITO/SnO_2/Perovskite/Spiro-OMeTAD/Au	25.12	1.17	83.86	24.61[25]
n-i-p	PEN/ITO/SnO_2/Perovskite/Spiro-OMeTAD/Au	24.91	1.2	81.79	24.51[26]
n-i-p	PEN/ITO/SnO_2/Perovskite/Spiro-OMeTAD/Au	25.69	1.184	83.59	25.42[27]
This work*	PEN/ITO/Ph-4PACz/Perovskite/C_{60}/BCP/Ag	24.51	1.186	84.41	24.54

References

1. G. Kresse and J. Furthmuller, *Phys. Rev. B*, 1996, **54**, 11169.
2. John P. Perdew, K. Burke and M. Ernzerhof, *Phys. Rev. Lett.*, 1996, **77**, 3865.
3. P. E. Blöchl, *Phys. Rev. B*, 1994, **50**, 17953.
4. S. Grimme, S. Ehrlich and L. Goerigk, *J. Comput. Chem.*, 2011, **32**, 1456-1465.
5. S. Grimme, J. Antony, S. Ehrlich and H. Krieg, *The Journal of Chemical Physics*, 2010, **132**, 154104.
6. Y. Zheng, Y. Li, R. Zhuang, X. Wu, C. Tian, A. Sun, C. Chen, Y. Guo, Y. Hua, K. Meng, K. Wu and C.-C. Chen, *Energy Environ. Sci*, 2023, **17**, 1153-1162
7. J. Zhou, L. Tan, Y. Liu, H. Li, X. Liu, M. Li, S. Wang, Y. Zhang, C. Jiang, R. Hua, W. Tress, S. Meloni and C. Yi, *Joule*, 2024, **8**, 1691-1706.
8. L. Qiuyang, L. Hong, H. Cheng-Hung, Y. Haoming, L. Shunde, C. Peng, X. Hongyu, Y. Wen-Yi, Z. Yiping, S. Yanping, Z. Qixuan, J. Yongqiang, S. Jing-Jong, J. Shuang, Y. Bo, T. Pengyi, G. Qihuang, Z. Lichen and Z. Rui, *Nat. Energy*, 2024, **9**, 1506–1516.
9. M. Li, B. Jiao, Y. Peng, J. Zhou, L. Tan, N. Ren, Y. Ye, Y. Liu, Y. Yang, Y. Chen, L. Ding and C. Yi, *Adv. Mater.*, 2024, **36**, 2406532.
10. H. Chen, C. Liu, J. Xu, A. Maxwell, W. Zhou, Y. Yang, Q. Zhou, A. S. R. Bati, H. Wan, Z. Wang, L. Zeng, J. Wang, P. Serles, Y. Liu, S. Teale, Y. Liu, M. I. Saidaminov, M. Li, N. Rolston, S. Hoogland, T. Filleter, M. G. Kanatzidis, B. Chen, Z. Ning and E. H. Sargent, *Science*, 2024, **384**, 189-193.
11. C. Liu, Y. Yang, H. Chen, J. Xu, A. Liu, A. S. R. Bati, H. Zhu, L. Grater, S. S. Hadke, C. Huang, V. K. Sangwan, T. Cai, D. Shin, L. X. Chen, M. C. Hersam, C. A. Mirkin, B. Chen, M. G. Kanatzidis and E. H. Sargent, *Science*, 2023, **382**, 810-815.
12. S. Yunxiu, Z. Tiankai, X. Guiying, A. S. Julian, C. Xiankai, C. Weijie, Z. Guanhaojie, L. Jiajia, G. Boyu, Y. Heyi, W. Yeyong, L. Xia, A. Thamraa, Y. Wanjian, Z. Jian, W. Feng, A. Aram, G. Xingyu, Z. Xiaohong, G. Feng, L. Yaowen and L. Yongfang, *Nature*, 2024, **635**, 882–889.
13. L. Yong, X. Zhuang, D. Yuwei, L. Yongzhe, S. Yiqiao, S. Chunbo, L. Hongxiang, S. Rui, C. Minghui, W. Hanye, X. Dongfang, Z. Ke, W. Yifan, L. Hongjie, P. Qiang, G. Kunpeng, L. Shengzhong and L. Zhike, *Adv. Mater.*, 2024, **9**, 2414354.
14. Y. Yi, C. Hao, L. Cheng, X. Jian, H. Chuying, D. M. Christos, W. Haoyue, S. R. B. Abdulaziz, W. Zaiwei, P. R. Robert, W. G. Isaiah, K. Shuta, E. W. Taylor, Z. Stefan, S. Selengesuren, B. Munkhbayar, X. C. Lin, C. Bin, G. K. Mercouri and H. S. Edward, *Science*, 2024, **386**, 898-902.
15. S. Liu, J. Li, W. Xiao, R. Chen, Z. Sun, Y. Zhang, X. Lei, S. Hu, M. Kober-Czerny, J. Wang, F. Ren, Q. Zhou, H. Raza, Y. Gao, Y. Ji, S. Li, H. Li, L. Qiu, W. Huang, Y. Zhao, B. Xu, Z. Liu, H. J. Snaith, N.-G. Park and W. Chen, *Nature*, 2024, **632**, 536–542.
16. G. Cheng, L. Haiyun, X. Zhiyuan, L. Yuheng, W. Huaxin, Z. Qixin, W. Awen, L. Zhijun, G. Zhihao, Z. Cong, W. Baiqian, L. Xiong and Z. Zhigang, *Nat. Commun.*, 2024, **15**, 9154.
17. Y. Wen, T. Zhang, X. Wang, T. Liu, Y. Wang, R. Zhang, M. Kan, L. Wan, W. Ning, Y. Wang and D. Yang, *Nat. Commun.*, 2024, **15**, 7085.
18. Z. Jie, L. Zhixin, W. Deng, W. Jiawen, Z. Peide, B. Yuqi, G. Xiaoyu, Q. Geping, H. Bihua, W. Xingzhu, Z. Yong, Y. Lei, K. Y. J. Alex and X. Baomin, *J. Am. Chem. Soc.*, 2024, **147**, 725–733.
19. X. Zhuang, D. Yuwei, C. Minghui, L. Yong, L. Zhike, L. Hongxiang, C. Yu, Z. Zhigang, L. Shengzhong and P. Qiang, *Angew. Chem. Int. Ed.*, 2024, **9**, 202419070.
20. X. Tong, L. Xie, J. Li, Z. Pu, S. Du, M. Yang, Y. Gao, M. He, S. Wu, Y. Mai and Z. Ge, *Adv. Mater.*, 2024, **36**, 2407032.

21. X. Chen, W. Cai, T. Niu, H. Wang, C. Liu, Z. Zhang, Y. Du, S. Wang, Y. Cao, P. Liu, W. Huang, C. Ma, B. Yang, S. Liu and K. Zhao, *Energy Environ. Sci*, 2024, **17**, 6256-6267
22. Y. Wu, G. Xu, Y. Shen, X. Wu, X. Tang, C. Han, Y. Chen, F. Yang, H. Chen, Y. Li and Y. Li, *Adv. Mater.*, 2024, **36**, 2403531.
23. C. Gong, C. Wang, X. Meng, B. Fan, Z. Xing, S. Shi, T. Hu, Z. Huang, X. Hu and Y. Chen, *Adv. Mater.*, 2024, **36**, 2405572.
24. L. Xie, S. Du, J. Li, C. Liu, Z. Pu, X. Tong, J. Liu, Y. Wang, Y. Meng, M. Yang, W. Li and Z. Ge, *Energy Environ. Sci*, 2023, **16**, 5423-5433
25. R. Xu, F. Pan, J. Chen, J. Li, Y. Yang, Y. Sun, X. Zhu, P. Li, X. Cao, J. Xi, J. Xu, F. Yuan, J. Dai, C. Zuo, L. Ding, H. Dong, A. K. Y. Jen and Z. Wu, *Adv. Mater.*, 2023, **36**, 2308039.
26. Y. Wang, Y. Meng, C. Liu, R. Cao, B. Han, L. Xie, R. Tian, X. Lu, Z. Song, J. Li, S. Yang, C. Lu and Z. Ge, *Joule*, 2024, **8**, 1120-1141.
27. W. Cong, G. Chenxiang, A. Wei, F. Baojin, M. Xiangchuan, S. Siyi, H. Xiaotian and C. Yiwang, *Adv. Mater.*, 2025, **9**, 2417779.